RSC Advances

PAPER

View Article Online
View Journal | View Issue

Cite this: *RSC Adv.*, 2022, **12**, 13660

Hydrogen bonds-triggered differential extraction efficiencies for bifenthrin by three polymeric ionic liquids with varying anions based on FT-IR spectroscopy

Xiaofan Zhang,†[a] Ming Gao,†[a] Tingting Liu,[b] Huili Wang[a] and Xuedong Wang *[a]

Herein, we fabricated three imidazolium-based polymeric ionic liquids (PILs) with different anions (P[VEIM]BF_4, P[VEIM]PF_6 and P[VEIM]Br), and analyzed their differential extraction efficiencies for bifenthrin through H-bonding induced effects. Three PILs all presented an irregular block structure with rough surface and lower specific-surface area (SSA, 11.2–18.7 m^2 g^{-1}) than carbon-based nanomaterials. They formed hydrogen bonds with free-water molecules in the lattice of PILs, including $C_{2,4,5}$–H···O–H, Br···H–O–H···Br, O–H···Br, $C_{2,4,5}$–H···F–P, P–F···H–O–H···F–P, $C_{2,4,5}$–H···F–B and B–F···H–O–H···F–B. After extraction, the O–H stretching-vibration peak was prominently intensified, whereas the C–H bond varied slightly concomitant with reduced B–F and P–F vibration. Theoretically, the C–H vibration should become more intense in the $C_{4,5}$–H···H_2O and C_2–H···H_2O bonds after extraction in contrast to before extraction. These contrary spectral changes demonstrated that the hydrogen bonds between cations in the PILs and free-water molecules were broken after extraction, yielding the H-bonding occurrence between bifenthrin and H–O–H in the lattice. As a time indicator for the free-water binding and releasing process, the highest slope for the plot of I_t/I_0 against time implied that the shortest time was required for P[VEIM]PF_6 to reach an adsorption equilibrium. Overall, the strong hydrophobicity, small SSA and electrostatic-repulsion force for P[VEIM]PF_6 are all not conducive to its efficient adsorption. Beyond our anticipation, P[VEIM]PF_6 provided the highest extraction recovery for bifenthrin up to 92.4% among three PILs. Therefore, these data lead us to posit that the above high efficiency results from the strongest H-bonding effect between P[VEIM]PF_6 and bifenthrin. These findings promote our deep understanding of PILs-triggered differential efficiency through a H-bonding induced effect.

Received 1st March 2022
Accepted 27th April 2022

DOI: 10.1039/d2ra01371a

rsc.li/rsc-advances

1. Introduction

Polymeric ionic liquids (PILs) possess the advantages of both ionic liquids (ILs) and polymers, and thus have good ionic and conductive properties,[1,2] which expand their applications as fit-for-purpose and functional ILs. Currently, two kinds of PILs have been widely reported: the first is that the polymerized groups are introduced into ILs to prepare functional PILs through polymerization; the second is that the composite metals or metal oxides with catalytic activity are integrated with PILs for the sake of fabricating supported PILs.[3–5] Lin and coworkers (2021) fabricated polymeric self-solidifying ionic liquids as catalysts for producing biodiesel under mild conditions with good recyclability.[3] Safa's group (2016) synthesized a series of PILs-based gel electrolytes, which were employed in lithium batteries and achieved higher catalytic efficiency than using ILs alone.[4] The aliphatic hydroxyl-functionalized imidazole PILs were used to catalyze CO_2-cycloaddition reaction of epoxides with high yields, and could be recycled many times with no significant decrease in their catalytic performance.[5] Peng *et al.* (2020) prepared many kinds of PIL-based microspheres as the stationary phase in HPLC columns and achieved satisfactory separation efficiency for organic pollutants.[6]

Also, PILs are extensively used in gas adsorption and separation, especially in CO_2 adsorption, which solve the bottleneck problem of ILs in high viscosity and low-adsorption selectivity.[7–9] Under the same experimental conditions, the PILs, based on 1-(4-vinylphenyl)-3-butyl-imidazole ILs, provided the adsorption capacity for CO_2 3–5-fold greater than that of ordinary imidazole ILs.[7,8] Xiong's group (2012) synthesized a type of PILs by introducing the IL groups into the main chain of a polymer, and observed that their adsorption capacity for CO_2 reached up to 10% with shorter adsorption–desorption equilibrium time.[9,10] Besides, PILs have been widely used in various

[a]*School of Environmental Science and Engineering, Suzhou University of Science and Technology, Suzhou 215009, China. E-mail: zjuwxd@163.com*

[b]*Jiangsu Provincial Key Laboratory of Environmental Science and Engineering, Suzhou University of Science and Technology, Suzhou 215009, China*

† Xiaofan Zhang and Ming Gao are the co-first authors.

nanocomposites. In common cases, nanomaterials easily lose the practical application value due to high specific surface area, which is dynamically unstable and shows strong agglomeration phenomenon. Therefore, stabilizers, such as surfactants and soluble polymers, are often added to nanomaterials to prevent the agglomeration of nanoparticles. Due to possessing polar ionic bonds and long spatial chain, PILs can stabilize nanoparticles by virtue of electrostatic and steric effects. Matandabuzo and Alibade synthesized vinyl-pyridinium PILs to further prepare the nanocomposites of PILs and multiwalled carbon nanotubes (PIL/MWCNT), which showed maximum adsorption capacity of 37% for Cr(VI) within 12 h agitation.[10] Based on 1-vinyl-3-methylimidazole chloride and *n*-vinyl-2-carbonylpyrrolidine, the as-synthesized copolymers were mixed with [BMIM]BF_4 and added to rhodium nanoparticles to improve the catalytic activity and lifetime.[11] Although several reports on the utilization of PILs have been reported as catalysts and adsorbents, there is a paucity of information regarding their applications as extractant in analytical pretreatment procedures. Enlightened by the aforementioned analyses, our group synthesized three kinds of imidazolium-based PILs with different anions (BF_4^-, PF_6^- and Br^-). In the lattice of PILs, many kinds of hydrogen bonds were found to be formed with free water molecules (Fig. 1). After adsorption/extraction of bifenthrin, the underlying mechanisms regarding differential extraction efficiencies were explored in detail by virtue of changes in the formation, reintegration and vibration of hydrogen bonds in PILs before and after extraction.

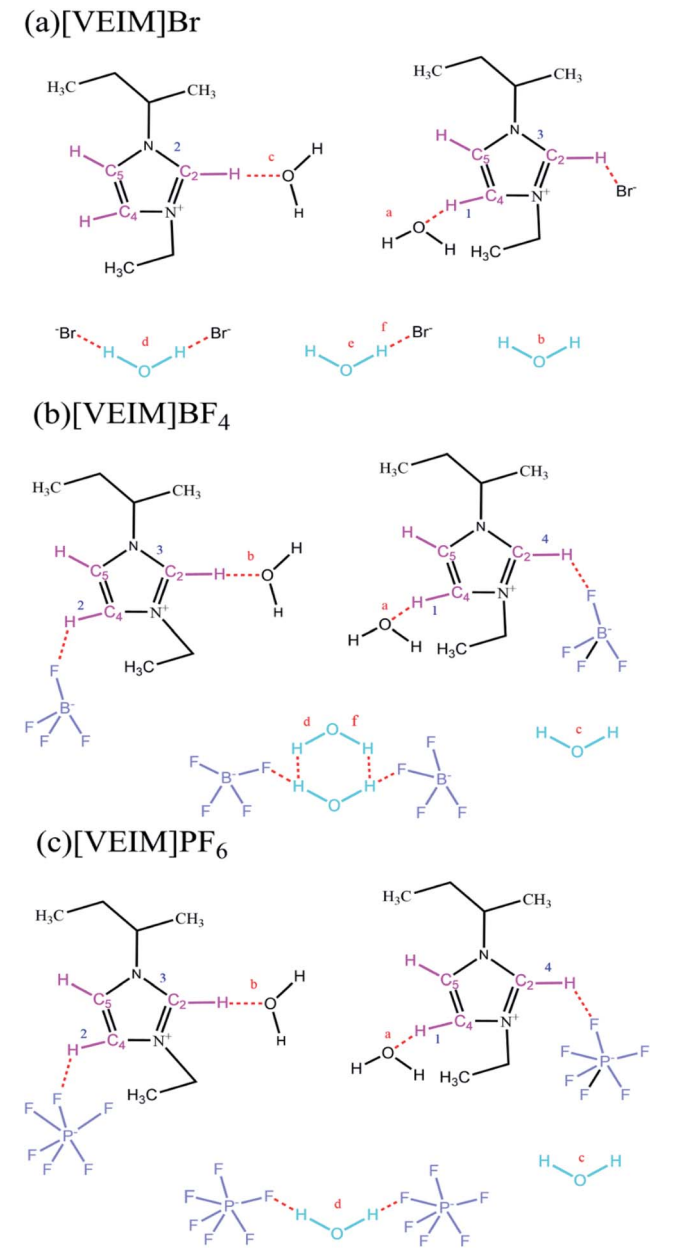

Fig. 1 Types of hydrogen bonds in the lattice of PILs. (a) P[VEIM]Br; (b) P[VEIM]BF_4, (c) P[VEIM]PF_6.

Among common pesticides, pyrethroids compounds are widely used to control agricultural/forestry insects all over the world due to high efficiency, rapidity, broad spectrum, and strong photostability. With the abuse increase of pyrethroids, they not only cause serious impact on the environment, but also accumulate excessive residues in fruits and vegetables, which affect central nervous system and lead to disturbance of consciousness.[12,13] The maximum residue limits (MRLs) of pyrethroids in foods have been set at 0.02 to 0.5 mg kg^{-1} in China (GB2763-2019), and 0.02 to 0.3 mg kg^{-1} in European Union (Part A of Annex to Reg. 396/2005), respectively.[14] Common analytical approaches for pyrethroids detection include GC-ECD, GC-MS, HPLC-DAD, and so on.[15] At present, the sample pretreatment methods for pyrethroids in complex matrices include liquid–liquid extraction, solid-phase extraction, magnetic solid-phase extraction, and so on.[16] However, owing to the presence of trace-level pyrethroids and various interference chemicals and ions, the rapid/sensitive assay of pyrethroids is still a challenging issue in environmental and food matrices.

Hydrogen bonds play crucial roles in determining the extraction efficiency of ILs for target analytes. Previous literature reported the effects of polymethylated imidazole cations, imidazole nitrogen cations and NTF_2^- anions on the properties of ILs (melting point and viscosity) by hydrogen bonds,[17] and also investigated the H-bonding role in crystal structure.[18] In typical imidazolium-based ILs, hydrogen bonds between cations and anions are considered to be the key factor to determine the microstructure and macroscopic properties. Hu and coworkers employed density functional theory (DFT) to illustrate the relationship between viscosity and hydrogen bonds in ILs.[19] Due to the H-bonding importance in determining IL's property and structure, there have been many reports on the dependence of ILs on H-bonding strength.[19–21] The optimized geometry of H-bonding ion pairs was predicted for imidazolium-based ILs with varying anions by DFT. Phadagi *et al.* and Liu *et al.* calculated the H-bonding strength changes of different cations and anions in PILs by FT-IR spectroscopy and DFT.[20,21]

As far as our information goes, no reports are related to the application of PILs for bifenthrin extraction as a model chemical in pyrethroids, the underlying H-bonding formation, and

reintegration mechanism in the extraction process. Motivated by the above issue, we prepared three kinds of imidazolium-based PILs with different anions, explored their interactions with bifenthrin, and confirmed the crucial roles of anions in the H-bonding occurrence. Prior to adsorption, the anions formed hydrogen bonds with free water molecules in the lattice of PILs. Three kinds of H-bonding forms existed in the carbon atoms of imidazolium ring: C_2–H, C_4–H and C_5–H.[22,23] Free water molecules interacted with anions of PILs by hydrogen bonds as $H_2O\cdots$anion and anion$\cdots H_2O\cdots$anion. Consequently, the formation and reintegration of O–H, C–H, P–F and B–F vibration peaks were investigated in detail by virtue of changes in FT-IR spectra before and after extraction. This work sheds new light on mechanistic insight into the differential extraction efficiencies for target analytes by PILs, resulting from the changes in H-bonding interactions between PILs and analytes.

2. Materials and methods

2.1. Reagents and chemicals

Bifenthrin with purity of 99.5% was purchased from the China Chemical Standard Corporation (Beijing, China), and its molecular structure is shown in Fig. 2a. *N*-Vinylimidazole (98.0%), and the analytical-grade bromoethane, sodium tetrafluoroborate, potassium hexafluorophosphate, and azobisisobutyronitrile (AIBN) were all obtained from Tansoole (Shanghai, China). Chromatographic-grade acetone, methanol, acetonitrile and ethyl acetate were sourced from Aladdin (Shanghai, China).

2.2. Instrumentation

The structures and morphologies of three PILs were characterized by a scanning electron microscopy (Zeiss Sigma 300, Germany; accelerating voltage 20.0 kV, working distance 9.8–10.2 mm, ETD detector). The gold coating of the SEM used an Agar Auto Sputter Coater mod. 108 (Cressington, UK), with purity > 99.99%, current 40 mA, and 30 s coating time. The FT-IR spectra of PILs were measured with a scanning range of 400–4000 cm^{-1} by the KBr method in a Bruker Tensor II infrared spectrometer (Brook, Germany). The spectral intensity ratios (I_t/I_0) reflect the situations on H-bonding breakage or reintegration, where I_t and I_0 denote the intensities of O–H or C–H bonds after adsorption in different time intervals and prior to adsorption, respectively. X-ray photoelectron spectroscopy (XPS) measurements were performed using a PHI Quantera spectrometer with Al Kα X-ray ($h\nu$ = 1486.6 eV) radiation. UV-Vis spectra were recorded on a UV-5500PC spectrophotometer (Metash, Malvern, UK). A SDT Q600 thermal gravimetric analyzer (PerkinElmer, MA, USA) was employed to analyze the thermal stability of PILs, and it was operated at a heating rate of 10 °C min^{-1} across the temperature range of 30–600 °C under a N_2 flow. The decomposed temperature was analyzed based on the weight-loss curves. Also, a Setsys Ev 24 model thermal analyzer (Setaram, Paris, France) was used to detect the glass transition temperature (T_g) according to differential scanning calorimetric curves over the temperature range of 150–300 °C. The Brunauer–Emmett–Teller (BET) surface area was measured by N_2 adsorption–desorption at 77 K using an ASAP 2020 System (Quantachrome, USA). Zeta potential was detected by a zeta potential analyzer (Malvern, UK). The measurement of solution pH was carried out using a Leici PHB-4 pH meter (Inesa Scientific Corporation, Shanghai, China). All stock and work solutions were prepared using ultrapure water (18.25 MΩ) from Hangzhou Jiejing Purification System (Hangzhou, China). The water-phase filter membrane (50 mm × 0.45 μm) was acquired from Tianjin Jinteng Experimental Equipment Corporation (Tianjin, China).

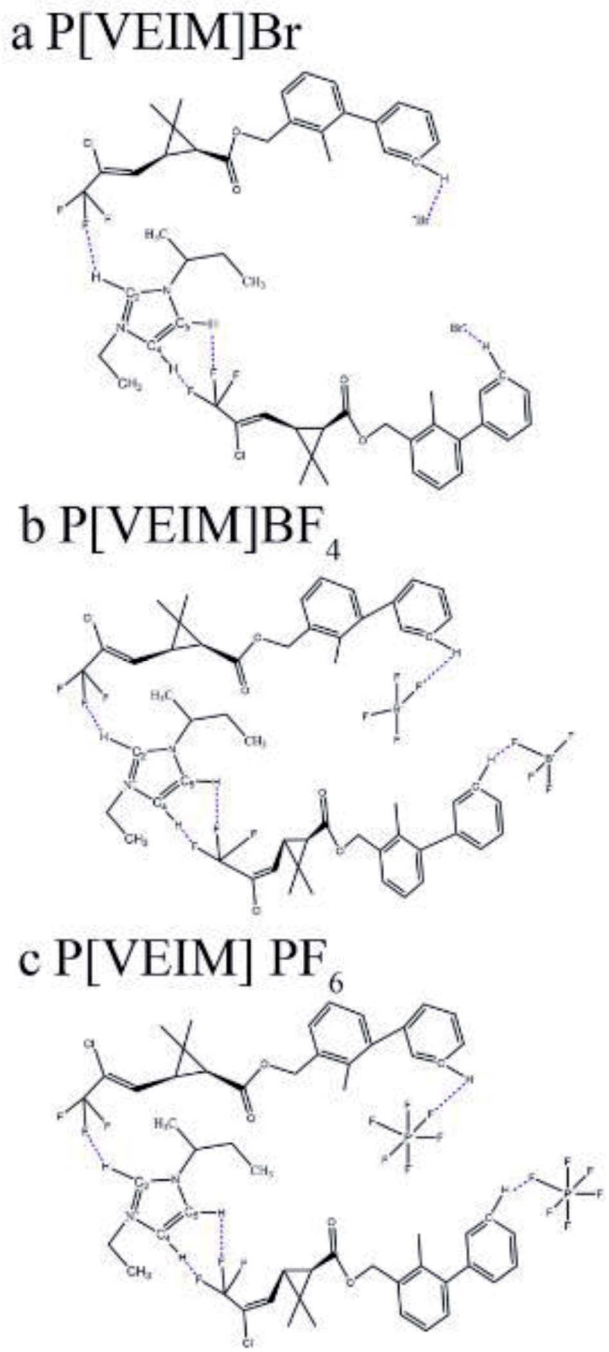

Fig. 2 Types of hydrogen bonds formed between PILs and bifenthrin. (a) The H-bonding types formed between P[VEIM]Br and bifenthrin; (b) the H-bonding types formed between P[VEIM]BF_4 and bifenthrin; (c) the H-bonding types formed between P[VEIM]PF_6 and bifenthrin.

2.3. Bifenthrin detection

The concentration of bifenthrin was determined by a Shimadzu LC-20AT liquid chromatography equipped with a diode-array detector (HPLC-DAD). Chromatographic separation was conducted on a Shim-Pack GIST C_{18} column (250 mm × 4 mm, 5 μm) under the following operational conditions: mobile phase, acetonitrile–water at 80% : 20% by v/v; flow rate, 1 mL min^{-1}; and column temperature, 30 °C. The detection wavelength was set at 210 nm, and the injection volume was 20 μL under a 10 μL sample loop. The differential extraction efficiencies for bifenthrin were assessed in the following optimized conditions: ultrapure water, 10 mL; the fortified bifenthrin level, 500 μg L^{-1}; solution pH, 7.0; and elution solvent, 1.2 mL methanol. Briefly, after 10 min ultrasonic adsorption, the PILs containing analytes were centrifuged at 5000 rpm for 5 min, and the supernatant was discarded. The settled phase was eluted by methanol and filtered by a 0.22 μL membrane filter, and the resultant eluent was subjected to HPLC-DAD analysis.

2.4. Fabrication of PILs

As vividly elaborated in Fig. 3, 0.05 mol of *N*-vinylimidazole was accurately weighed and added to a 100 mL round-bottom flask

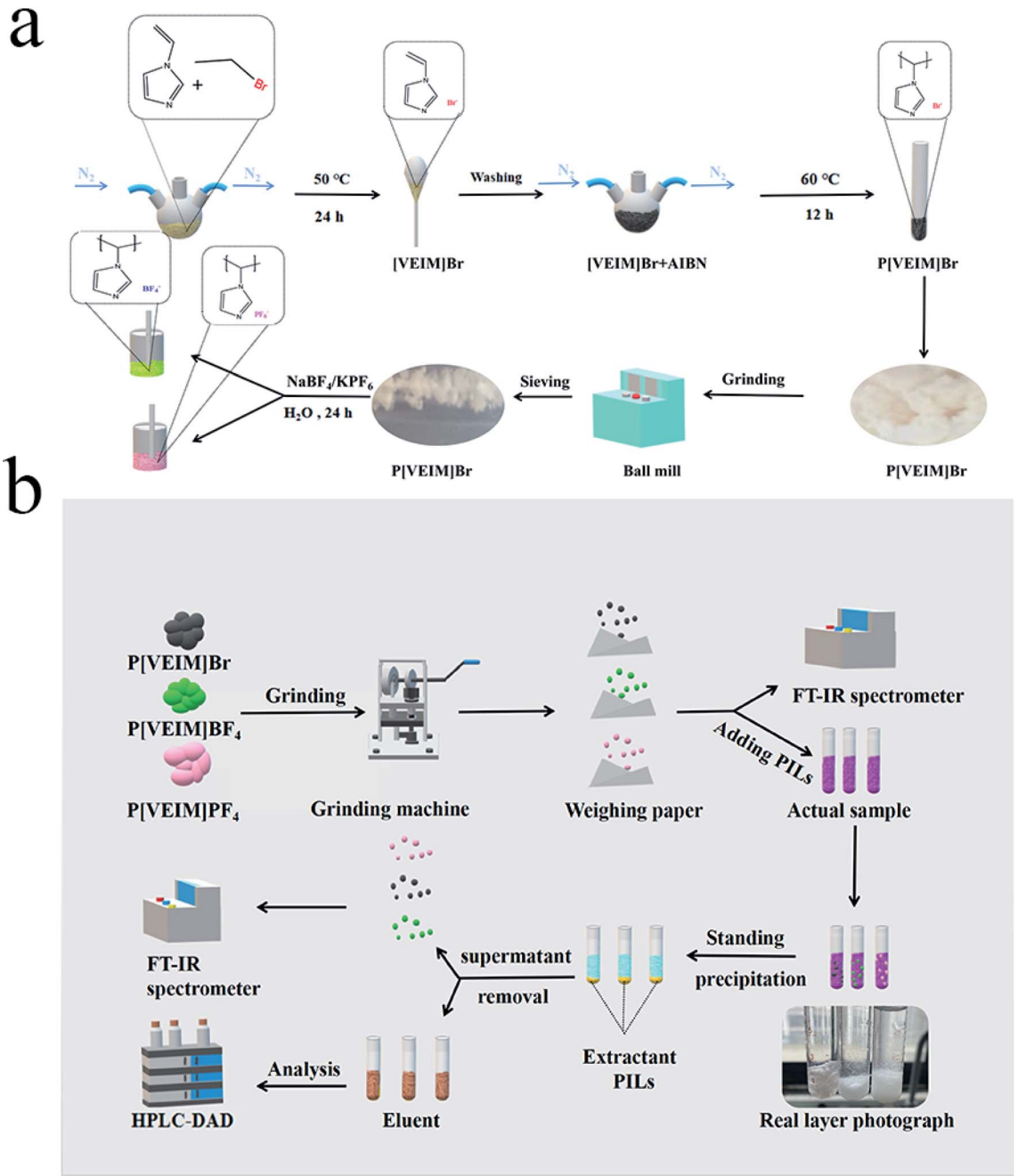

Fig. 3 Schematic diagram of the preparation (a) and adsorption/extraction (b) processes by PILs.

under N_2 protection, and then 0.10 mol of bromoethane was added dropwise to the above flask and refluxed for 24 h at 50 °C. With increasing reaction time, the solution viscosity continued to rise to form a yellow-white solid product, which was further washed three times with ethyl acetate to remove an excessive reaction precursor and dried in a vacuum drying oven for 24 h. Finally, ~8.4 g of the product was obtained with a yield of 82.2%. Upon addition of an initiator AIBN, ILs monomer [VEIM]Br with double bond was polymerized to form P[VEIM]Br. To be more precise, 6.14 g of [VEIM]Br, 0.08 g of AIBN, and 35 mL of chloroform were added to a 100 mL round-bottom flask, protected by N_2 flow and reacted under reflux conditions at 50 °C. When the reaction solution was relatively stable, it was kept at 60 °C for 12 h reaction. Clearly, a yellow-white solid were gradually formed in the solution, and as the reaction continued, the resultant precipitate gradually became bulk solid. After the reaction, the precipitate was washed three times with chloroform, and the product obtained was vacuum-dried at 40 °C. Finally, 5.75 g of the yellow-white solid was achieved with a yield as high as 93.7%. Subsequently, other two kinds of PILs (P[VEIm]BF_4 and P[VEIm]PF_6) were prepared by virtue of anion exchanging reaction. Briefly, 5.30 g of P[VEIM]Br, and 5.50 g of $NaBF_4$ for P[VEIM]BF_4 (or 5.00 g of KPF_6 for P[VEIM]PF_6) were added to a 100 mL single-neck flask and stirred for 12 h at ambient conditions. After the reaction, the resultant precipitate was filtered and vacuum-dried at 60 °C for 6 h. The final bulk solid was ground into powder, washed with ultrapure water for three times, and further vacuum-dried for 6 h. The as-achieved yellow-white solid for P[VEIM]BF_4 or P[VEIM]PF_6 was employed in the following trials.

2.5. FT-IR spectra of PILs before and after extraction

After the bulk solids of three PILs were ground into powder, aliquots of them were subjected to FT-IR analyses, which were referred to as the sample before extraction. After an appropriate time of adsorption, the PILs containing bifenthrin were eluted with methanol as described in Section 2.3, vacuum-dried for 6 h and subjected to FT-IR detection as the sample after extraction (Fig. 3b). For peak deconvolution, the FT-IR spectra were fitted with the Voigt function using the Origin 8.0 software. In such cases, the chi-squared value for each fitting curve was more than 0.99 in the deconvolution. As for the FT-IR spectra of PILs with varying anions, we focused on observation on the O–H stretching band at 3100–3700 cm^{-1}, C–H stretching band at 2700–3200 cm^{-1}, and B–F stretching band at 950–1152 cm^{-1}, respectively.[24–26] Based on changes in the above stretching bands, the H-bonding occurrence and reintegration information in PILs were deducted before and after extraction.

3. Results and discussion

3.1. Characterization of three PILs with varying anions

3.1.1. SEM images of three PILs. Fig. 4 shows the SEM images of P[VEIM]Br, P[VEIM]BF_4, and P[VEIM]PF_6 at 10 000× magnification. Obviously, the imidazolium-based PILs with varying anions displayed the similar morphology. They presented irregular and asymmetric block structure with rough surface and no fixed crystal shape. From the overall appearance, PILs were close to the shape of jade and pile up with different sizes of particles, demonstrating the formation of amorphous polymers.[27]

3.1.2. TGA analyses of PILs. As shown in Fig. 5a, the TGA curves of P[VEIM]BF_4, P[VEIM]PF_6, and P[VEIM]Br were mainly divided into two stages. For the first stage of P[VEIm]BF_4, the weight loss was <15% below 300 °C, which resulted from the loss of water. For the second stage, the weight loss was >75% at 300–440 °C, resulting from the decomposition of the polymer framework. As for P[VEIm]PF_6, only ~10% of the weight loss was observed below 280 °C, indicating the less water content in this PIL; in sharp contrast, the weight loss was >80% at 280–430 °C, which was attributable to the decomposition of polymer backbone. For P[VEIm]Br, the weight loss was ~50% at 310 °C, illustrating an excessive water content due to its strong hydrophilicity. The weight loss of >80% at 310–400 °C was mainly caused by the framework decomposition of PILs. Collectively, the main weight loss of three PILs all occurred above 275 °C, demonstrating that the framework structure of as-fabricated PILs had good thermal stability. Relatively, the thermal stability of three PILs was in the following order: P[VEIm]PF_6 > P[VEIm]BF_4 > P[VEIm]Br. These findings demonstrate that the thermal stability of PILs is closely dependent on their hydrophobic–hydrophilic characteristics.

3.1.3. Glass transition temperature (T_g) by differential scanning calorimeter (DSC). The DSC curves of three PILs are shown in Fig. 5b, from which the T_g values were observed to be

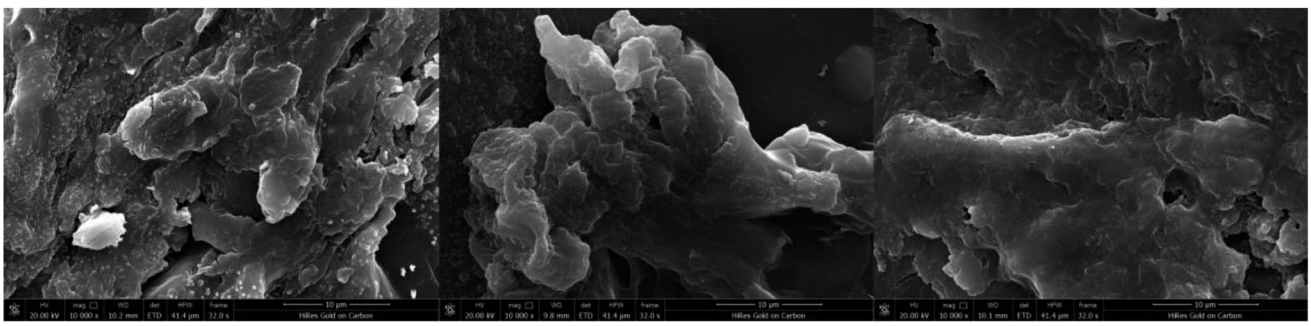

Fig. 4 The SEM images of three PILs (from left to right: P[VEIM]BF_4, P[VEIM]Br and P[VEIM]PF_6).

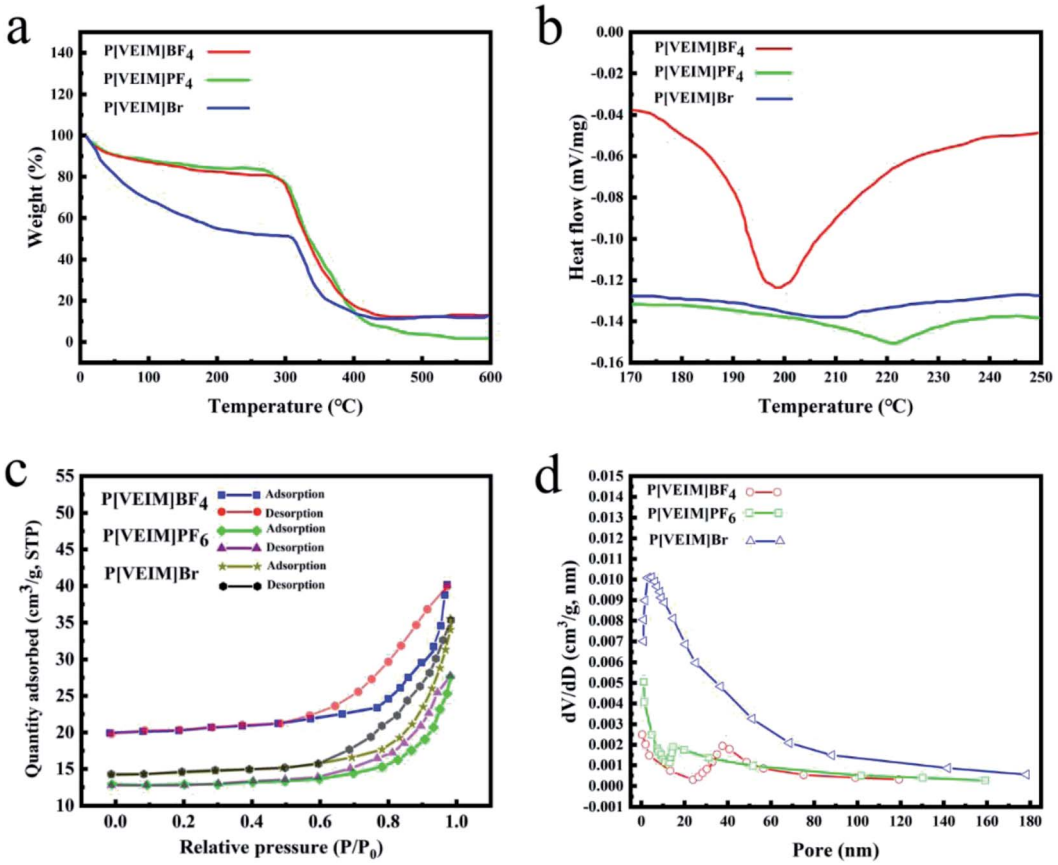

Fig. 5 Characterization of PILs. (a) TGA; (b) DSC; (c) N_2 adsorption–desorption curves; (d) distribution of pore size.

223, 200 and 205 °C for P[VEIm]PF_6, P[VEIm]BF_4 and P[VEIM]Br, respectively. Worth noting, no melting peaks occurred in three DSC curves, implying that they were all amorphous polymers.

3.1.4. BET specific surface area (SSA) and pore size. By means of analyses on N_2 adsorption–desorption curves, the BET SSAs of P[VEIM]BF_4, P[VEIM]PF_6 and P[VEIM]Br were calculated to be 18.7, 11.2 and 14.5 $m^2\ g^{-1}$, respectively (Fig. 5c). Their average pore size was 21.2 nm for P[VEIM]BF_4, 10.1 nm for P[VEIM]Br, and 11.2 nm for P[VEIM]PF_6, respectively, which all fell within the range of mesopore size (2–50 nm) (Fig. 5d). As compared to the reported carbon-based nanomaterials (SSAs of 100–600 $m^2\ g^{-1}$),[28] their smaller SSAs and mesoporous structure did not contribute to a large extent to the highly efficient adsorption of bifenthrin in aqueous phase.

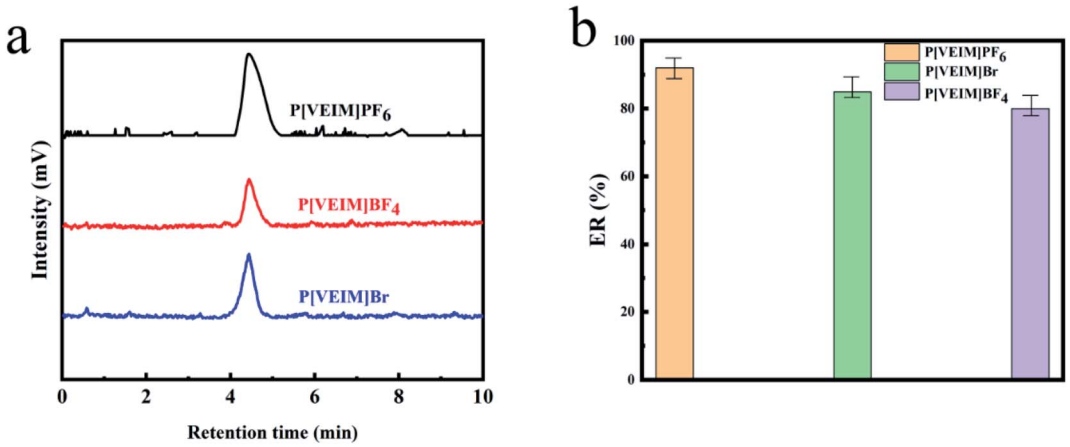

Fig. 6 Differential extraction efficiencies for bifenthrin by three PILs. (a) Typical HPLC-DAD chromatograms of bifenthrin after extraction by PILs; (b) average extraction recoveries for bifenthrin by PILs.

3.2. Differential extraction efficiency for bifenthrin by PILs

Under optimized experimental conditions (10 mL of ultrapure water, 500 μg L^{-1} of bifenthrin, solution pH, 7.0, and 1.2 mL methanol as elution solvent), we compared the extraction efficiencies of three PILs for bifenthrin. Fig. 6a shows the typical HPLC-DAD chromatograms of bifenthrin after extraction by PILs. The retention time of bifenthrin was observed at ~4.5 min. As displayed in Fig. 6, the average extraction recoveries (ERs) for bifenthrin were 92.4% by P[VEIM]PF_6, 85.3% by P[VEIM]Br, and 79.4% by P[VEIM]BF_4, respectively. Obviously, P[VEIM]PF_6 provided the highest ER for bifenthrin among three PILs, which were ~13.0% higher than that by P[VEIM]BF_4. The extraction efficiency for analytes by PILs is dependent on several factors, including the physico-chemical properties of PILs (SSA, zeta potential, pore size and so on), as well as the molecular interactions between PILs and analytes

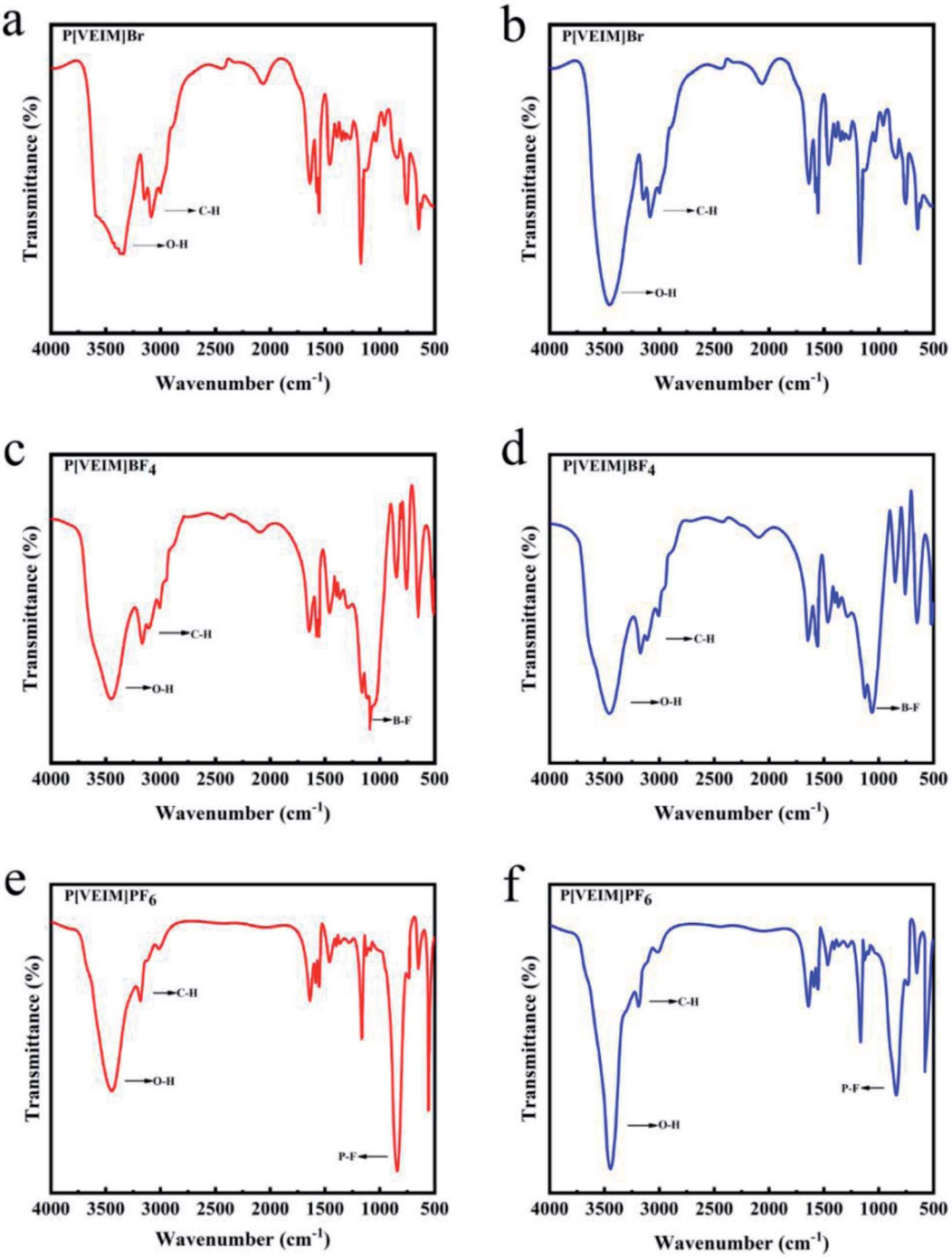

Fig. 7 FT-IR spectral changes before and after extraction. (a and b) Before and after extraction by P[VEIM]Br; (c and d), before and after extraction by P[VEIM]BF_4; (e and f) before and after extraction by P[VEIM]PF_6.

(hydrogen bond, π–π interaction and van der Waals force, and so on).[29] In the following experiments, we focused on unveiling the H-bonding changes before and after extraction and its relationship with PILs bearing with different anions.

3.3. H-bonding changes before and after extraction based on FT-IR spectra

Three PILs with imidazolium frameworks and varying anions were employed to analyze the FT-IR changes in hydrogen bonds before and after extraction (Fig. 7). P[VEIM]Br formed hydrogen bonds with free water molecules in the lattice of PILs, and the main types of hydrogen bonds were $C_{2,4,5}$–H···O–H, Br^-···H–O–H···Br^-, and O–H···Br^-.[30,31] As for P[VEIm]PF_6, the H-bonding forms were $C_{2,4,5}$–H···O–H, $C_{2,4,5}$–H···F–P, and P–F···H–O–H···F–P. With respect to P[VEIm]BF_4, the main hydrogen bonds concerned were $C_{2,4,5}$–H···O–H, $C_{2,4,5}$–H···F–B, and B–F···H–O–H···F–B.

The FT-IR spectra before and after extraction of bifenthrin are elaborated in Fig. 7a and b for P[VEIm]Br, Fig. 7c and d for P[VEIM]BF_4, and Fig. 7e and f for P[VEIM]PF_6, respectively. The vibration intensity of O–H reflected the absorption value of this bond in the FT-IR spectrum. For P[VEIM]Br, the O–H stretching-vibration peak at 3450 cm^{-1} was prominently intensified, whereas the C–H vibration at 3175 cm^{-1} varied slightly. As for P[VEIM]BF_4, two peaks were observed to change significantly before and after extraction, which showed the intensified O–H vibration at 3495 cm^{-1} and decreased B–F vibration at 1190 cm^{-1}, respectively. With regard to P[VEIM]PF_6, the O–H vibration peak at 3490 cm^{-1} was prominently increased; in sharp contrast, the P–F vibration at 895 cm^{-1} was substantially decreased. In contrast to the FT-IR spectra before and after extraction, no remarkable variations were observed for the C–H vibration peaks at 3200 cm^{-1} for P[VEIM]BF_4 and at 3270 cm^{-1} for P[VEIM]PF_6, respectively.

Prior to extraction, the hydrogen bonds formed between the anions and free water in the grids of PILs limited the vibrations of O–H, C–H, P–F, and B–F. However, the stretching vibrations of the O–H absorption band were significantly enhanced after extraction, providing compelling evidence for the breakage of hydrogen bonds between anions and free water molecules in the PILs. As well known, many kinds of molecular forces exist between adsorbents and target analytes. From the theoretical point of view, C–H, P–F, and B–F should vibrate more strongly after adsorption, while the opposite consequence was observed. Besides, the corresponding shrinking of three characteristic peaks in the FT-IR spectra further proved that the anions in the PILs and bifenthrin formed stronger hydrogen bonds to limit or bind the vibrations of C–H, P–F, and B–F.

As described above, hydrogen bonds formed by virtue of PF_6^-, BF_4^-, Br^- in PILs as receptors and hydrogen atoms in water molecules and on imidazolium ring as donors, respectively. Owing to the overlapping phenomenon of different O–H/C–H vibrations in total band, we deconvoluted the O–H/C–H peaks (3000–3800 cm^{-1}) of three PILs for the sake of illustrating the detailed FT-IR spectral changes before and after extraction.

3.4. Strong H-bonding production between PILs and bifenthrin by XPS analysis

As summarized in Table 1, the stretching vibrations could be deconvoluted into four peaks for C–H, and six peaks for O–H,[32–35] respectively. For P[VEIM]Br, five types of hydrogen bonds could form, which included H_2O···Br^-, Br^-···H_2O···Br^-, H_2O···$C_{4(5)}$–H, H_2O···C_2–H, and C_2–H···Br^-.[36,37] As similar as P[VEIM]Br, P[VEIM]BF_4 could yield five H-bonding categories: H_2O···BF_4^-, BF_4^-···H_2O···BF_4^-, H_2O···$C_{4(5)}$–H, H_2O···C_2–H, and C_2–H···BF_4^-.[38] Likely, the following hydrogen bonds could occur in the homogeneous solution of P[VEIM]PF_6, which were composed of H_2O···PF_6^-, PF_6^-···H_2O···PF_6^-, H_2O···$C_{4(5)}$–H, H_2O···C_2–H, and C_2–H···PF_6^-. After extraction, the O–H stretching-vibration band was remarkably intensified in the P[VEIM]Br, which possibly resulted from fracture of the H_2O···Br^-, Br^-···H_2O···Br^-, H_2O···$C_{4(5)}$–H, H_2O···C_2–H bonds in the lattice of PILs. By XPS analyses of P[VEIM]Br, the O–H stretching vibrations for H_2O···$C_{4(5)}$–H, H_2O···C_2–H and H–O–H became intense to a large extent; in stark contrast, the C–H vibrations for H_2O···$C_{4(5)}$–H and H_2O···C_2–H were evidently decreased, which implied the H-bonding breakage of $C_{4(5)}$–H···H_2O and C_2–H···H_2O after extraction (Fig. 8a and b). From a theoretical point of view, the C–H vibration should become more intense in the $C_{4(5)}$–H···H_2O and C_2–H···H_2O bonds after extraction when compared to before extraction. These contrary spectral changes provide compelling evidence that after extraction, the hydrogen bonds between cations in the PILs and free water molecules were broken, further resulting in the H-bonding occurrence between bifenthrin and H–O–H in the lattice of PILs.

Table 1 The decomposition of FT-IR peaks for three PILs[a]

	C–H				O–H	
Bonds no.	P[VEIM]PF_6	P[VEIM]BF_4	P[VEIM]Cl	Bonds no.	P[VEIM]PF_6	P[VEIM]Cl
1	3176	3169	3149	a	3676	3583
2	3160	3155	3104	b	3600	3537
3	3125	3123	3078	c	3594	3494
4	3118	3102	3030	d	3472	3405
				e		3322
				f		3248

[a] The H-bonding no. "1–2" and "a–f" are elaborated in Fig. 1.

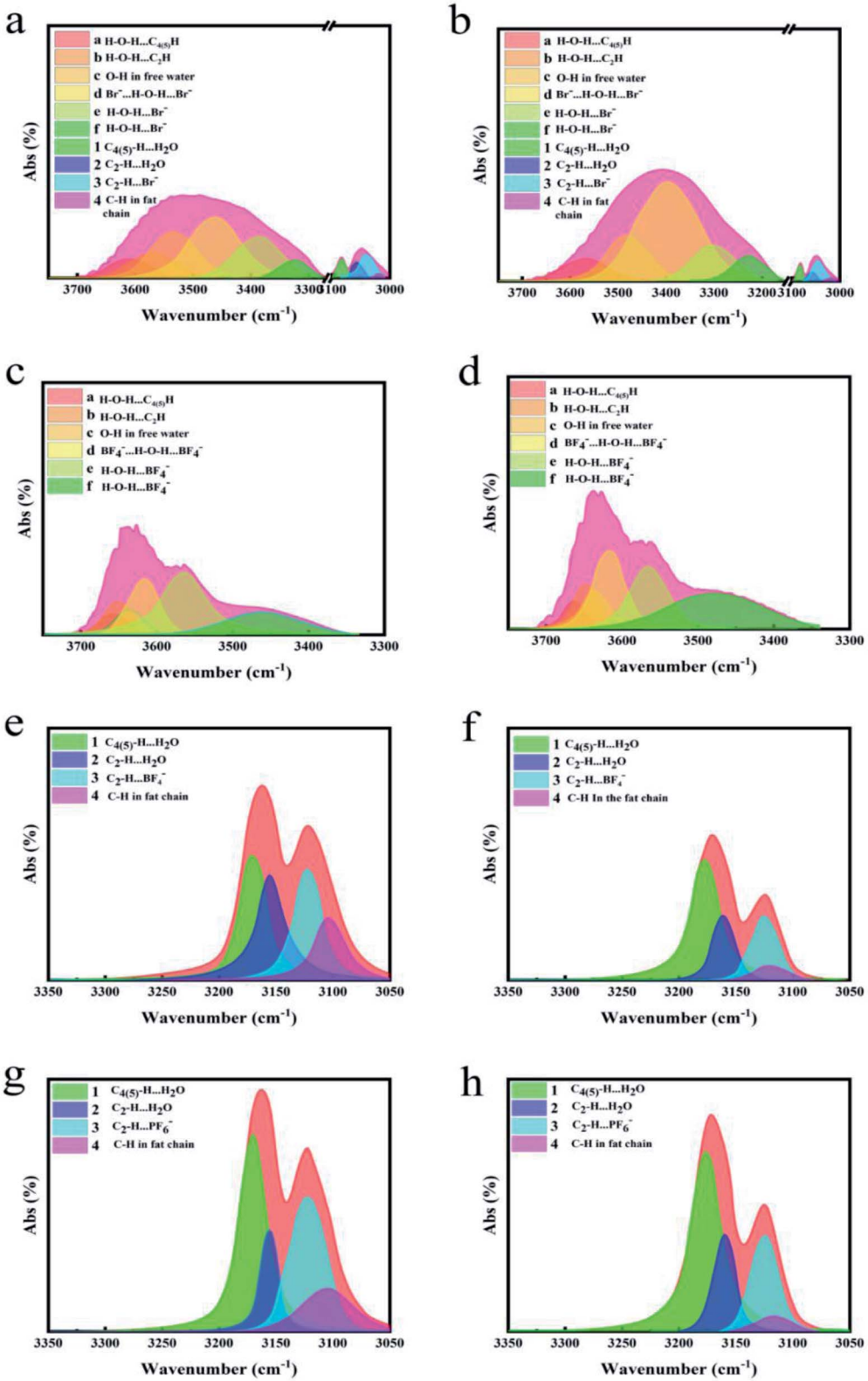

Fig. 8 XPS analyses on the C–H and O–H spectra before and after extraction. (a and b), C–H and O–H spectra before and after extraction by P[VEIM]Br; (c and d), O–H spectra before and after extraction by P[VEIM]BF_4; (e and f), C–H spectra before and after extraction by P[VEIM]BF_4; (g and h), C–H spectra before and after extraction by P[VEIM]PF_6.

After extraction, more intense O–H vibration and weaken B–F bond were observed in the lattice of P[VEIM]BF_4 as compared to before extraction (Fig. 8c and d). By XPS analysis, the following hydrogen bonds were confirmed to be fractured: $H_2O\cdots BF_4^-$, $BF_4^-\cdots H_2O\cdots BF_4^-$, $H_2O\cdots C_{4(5)}$–H, $H_2O\cdots C_2$–H, C_2–H$\cdots BF_4^-$ (Fig. 8).[39] Theoretically, more strong vibration of C_2–H$\cdots H_2O$, $C_{4(5)}$–H$\cdots H_2O$ and B–F bonds should occur after extraction of bifenthrin; with regret, the as-anticipated cases did not occur, demonstrating the stronger H-bonding occurrence between P[VEIM]BF_4 and bifenthrin after extraction. Similarly, in the FT-IR spectra of P[VEIM]PF_6, the O–H vibration at 3490 cm^{-1} became more intense, but the contrary changing trend was observed for P–F vibration at 895 cm^{-1} after extraction. Based on XPS analysis, a series of H-bonding strength was observed to be prominently weakened, including $C_{4,5}$–H$\cdots H_2O$, C_2–H$\cdots H_2O$, C_2–H$\cdots PF_6^-$ and C–H in the imidazolium ring (Fig. 8g and h), which displayed the contrary trends as those for the O–H vibration in Fig. 8e and f. These phenomena provide compelling evidence that the distinct H-bonding changes occur, and more intense hydrogen bonds form between PILs and bifenthrin in the extraction process.

3.5. Quantitative changes in the O–H vibration intensity of PILs before and after extraction

The H-bonding emergence mainly occurred at the positions of C_2, C_4, and anions (Br^{1-}, PF_6^{1-}, BF_4^{1-}) on the imidazolium ring of PILs. As illustrated in Fig. 9a, I_0 is the O–H vibration intensity prior to extraction, while I_t indicates that after extraction at varying extraction time. The ratio of I_t to I_0 (I_t/I_0) represents the binding and releasing processes of free water molecules by virtue of the breakage and reintegration of hydrogen bonds in the lattice of PILs.[40] The gradual increases in the I_t/I_0 values result from the breakage of hydrogen bonds between PILs and free water molecules. When rising up to a certain value, the I_t/I_0 ratios do not change because the extraction process reaches an equilibrium, and then it gradually decreases and returns to an original level.[40] The above changing trend for the I_t/I_0 values may be explained by the recyclability of PILs, which also proves the breakage and reintegration of hydrogen bonds on the PILs during the extraction process. For the plot of I_t/I_0 *vs.* time, the linear slopes of P[VEIM]BF_4, P[VEIM]PF_6 and P[VEIM]Br are 0.018, 0.013 and 0.12, respectively, suggesting that the shortest time is required for P[VEIM]PF_6 to reach an adsorption equilibrium.

3.6. Zeta potential changes of PILs before and after extraction

The zeta potentials of three PILs at varying solution pH are shown in Fig. 9b. When the solution pH spanned the range of 4.0–5.0, three PILs were all negatively charged from −28.7 mV to −10.2 mV. However, with further increases in solution pH from 6.0 to 8.0, the zeta potentials became positive for P[VEIM]Br and P[VEIM]BF_4 with exception of P[VEIM]PF_6. Under the optimized extraction conditions (pH = 6.0), P[VEIM]PF_6 was negatively charged (−12.7 mV), while P[VEIM]BF_4 and P[VEIM]Br were positively charged (9.6 and 10.7 mV). Similarly, the bifenthrin was negatively charged (−3.9 mV) under the solution pH of 6.0. As a consequence, there was electrostatic attraction between P[VEIM]Br and P[VEIM]BF_4 and bifenthrin besides the hydrogen-bonding effect, whereas a repulsive force occurred between P[VEIM]PF_6 and bifenthrin. As mentioned above, the P[VEIM]PF_6 gave the highest extraction efficiency (92.4%) for bifenthrin among three PILs. Building upon the above data analysis, we posit that the highest extraction efficiency of P[VEIM]PF_6 for bifenthrin mainly resulted from its stronger hydrogen-bonding effect in spite of the occurrence of a repulsive action.

3.7. Mechanistic understanding of the strongest H-bonding form between P[VEIM]PF_6 and bifenthrin

In common cases, the hydrophobicity of PILs may affect the H-bonding production speed and strength.[41,42] For three imidazolium-based PILs, the hydrophobic orders of their anions are PF_6^- > BF_4^- > Br^-. For P[VEIM]PF_6, it forms hydrogen bonds with bifenthrin mainly through cations because its smaller SSAs and mesoporous structure are

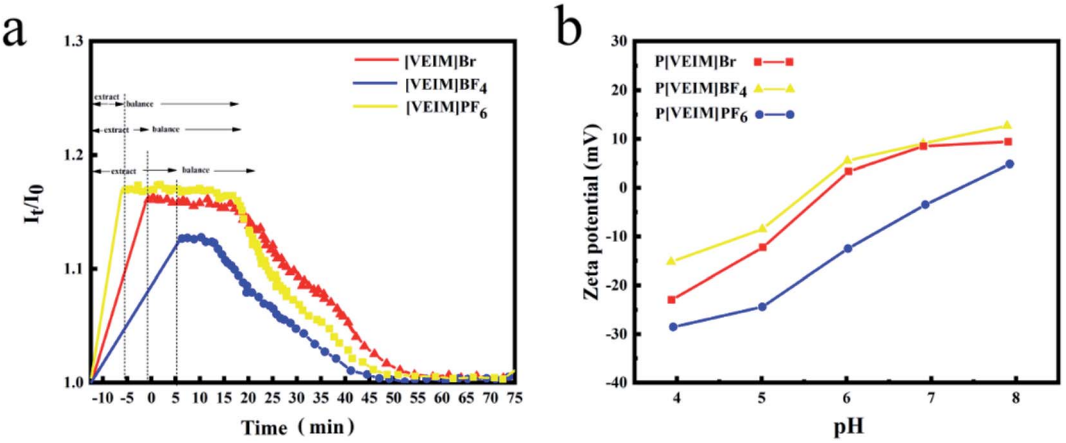

Fig. 9 (a) The formation and reintegration of hydrogen bonds; (b) zeta potential of PILs at varying solution pH. I_0 indicates the O–H vibration intensity before extraction; and I_t denotes the O–H vibration intensity at t time after extraction by PILs.

unfavorable for highly efficient adsorption of bifenthrin. In terms of electrostatic attraction, when the solution pH is 7.0, both P[VEIM]BF_4 and P[VEIM]Br are negatively charged, which are opposite to the charge of bifenthrin (Fig. 9b). Thus, we posit that electrostatic attraction existed between P[VEIM]BF_4 or P[VEIM]Br and bifenthrin.

In sharp contrast, P[VEIM]PF_6 has strong hydro P[VEIM]BF_4 or P[VEIM]Br and bifenthrin. The above analyses demonstrate that in the process of adsorption, P[VEIM]BF_4 and P[VEIM]Br not only form strong hydrogen bonds with target analytes, but also strong electrostatic attraction force exists between them. Due to strong hydrophobicity and small pore size in the P[VEIM]PF_6, both of the characteristics are not conducive to its dispersion in aqueous phase and efficient adsorption for target adsorbates. When the solution pH is 7.0, both P[VEIM]PF_6 and bifenthrin are negatively charged. Consequently, when P[VEIM]PF_6 adsorbs bifenthrin, the H-bonding form between them needs to overcome the electrostatic repulsion force in order to acquire a high extraction efficiency. Among three PILs, P[VEIM]PF_6 offers the highest extraction efficiency for bifenthrin up to 92.4%. Building upon the above analyses, we conclude that P[VEIM]PF_6 forms the strongest hydrogen bond with bifenthrin during the extraction.

4. Conclusion

In this investigation, we synthesized three imidazolium-based PILs with different anions (BF_4^-, PF_6^-, and Br^-) by employing *N*-vinyl group as a cross-linker and AIBN as an initiator. The morphologies and physical–chemical properties of three PILs were characterized/analyzed in detail by virtue of spectral techniques and several metrics, including SEM, FT-IR, TGA, N_2 adsorption–desorption and glass transition temperature (T_g). After extraction, the O–H stretching-vibration peak (3450–3500 cm^{-1}) was significantly intensified, whereas the C–H peak ($\sim$3100 cm^{-1}) remained nearly unchanged in concomitant with prominently decreased B–F (1190 cm^{-1}) and P–F (895 cm^{-1}) bonds. These spectral changes provide compelling evidence that after extraction, the hydrogen bonds between cations in the PILs and free water molecules were broken, further resulting in the H-bonding occurrence between bifenthrin and H–O–H in the lattice of PILs. For the plot of I_t/I_0 *vs.* time, the linear slopes of P[VEIM]BF_4, P[VEIM]PF_6 and P[VEIM]Br were 0.018, 0.013 and 0.12, respectively, suggesting that the shortest time was required for P[VEIM]PF_6 to reach an adsorption equilibrium. Because the following properties of P[VEIM]PF_6 (strong hydrophobicity, small SSA and electrostatic repulsion force) were all not beneficial to its efficient adsorption, it gave the highest extraction efficiency for bifenthrin up to 92.4% among three PILs. As such, it can be concluded that P[VEIM]PF_6 forms the strongest hydrogen bond with bifenthrin to achieve its high efficiency in the extraction process.

Conflicts of interest

The authors declare no conflict of interest.

Acknowledgements

This work was jointly supported by the National Science Foundation of China (22076134 and 21876125), Jiangsu Provincial Natural Science Foundation (BK20211338), Key Science & Technology Project of Suzhou City (SS202028), and Postgraduate Research & Practice Innovation Program of Jiangsu Province (KYCX20_2781).

References

1 G. Durga, P. Kalra, V. K. Verma, K. Wangdi and A. Mishra, Ionic liquids: from a solvent for polymeric reactions to the monomers for poly(ionic liquids), *J. Mol. Liq.*, 2021, **335**, 116540.
2 X. Lin, Y. Huang, L. Li, C. Ye, J. Chen and T. Qiu, Polymeric ionic liquids (PILs) with high acid density: tunable catalytic performance for biodiesel production, *Chin. J. Chem. Eng.*, 2021, **38**, 266–275.
3 X. Lin, M. Li, Z. Chen, M. Li, Y. Huang and T. Qiu, One-step fabrication of polymeric self-solidifying ionic liquids as the efficient catalysts for biodiesel production, *J. Cleaner Prod.*, 2021, **292**, 125967.
4 M. Safa, A. Chamaani, N. Chawla and B. El-Zahab, Polymeric ionic liquid gel electrolyte for room temperature lithium battery applications, *Electrochim. Acta*, 2016, **213**, 587–593.
5 S. Muhammad, M. N. Javed, F. I. Ali, A. Bari and I. A. Hashmi, Supramolecular polymeric aggregation behavior and its impact on catalytic properties of imidazolium based hydrophilic ionic liquids, *J. Mol. Liq.*, 2020, **300**, 112372.
6 Q. Peng, Y. Wu, H. Cong, Y. Shen, K. Mahmood and B. Yu, Preparation of monodisperse porous polymeric ionic liquid microspheres and their application as stationary phases for HPLC, *Talanta*, 2020, **208**, 120462.
7 A. Eftekhari and T. Saito, Synthesis and properties of polymerized ionic liquids, *Eur. Polym. J.*, 2017, **90**, 245–272.
8 S. Y. Zhang, Q. Zhuang, M. Zhang, H. Wang, Z. Gao, J.-K. Sun and J. Yuan, Poly(ionic liquid) composites, *Chem. Soc. Rev.*, 2020, **49**, 1726–1755.
9 G. Mittal, V. Dhand, K. Y. Rhee, S. J. Park and W. R. Lee, A review on carbon nanotubes and graphene as fillers in reinforced polymer nanocomposites, *J. Ind. Eng. Chem.*, 2015, **21**, 11–25.
10 M. Matandabuzo and P. A. Alibade, Vinyl pyridinium polymeric ionic liquid functionalized carbon nanotube composites as adsorbent for chromium(VI) in aqueous solution, *J. Mol. Liq.*, 2019, **196**, 111778.
11 X. L. Meng, Y. Nie, J. Sun, W. G. Cheng, J. Q. Wang, H. Y. He and S. J. Zhang, Functionalized dicyandiamide-formaldehyde polymers as efficient heterogeneous catalysts for conversion of CO_2 into organic carbonates, *Green Chem.*, 2014, **16**, 2771–2778.
12 S. Chen, S. Gu, Y. Wang, Y. Yao, G. Wang, Y. Jin and Y. Wu, Exposure to pyrethroid pesticides and the risk of childhood brain tumors in East China, *Environ. Pollut.*, 2016, **218**, 1128–1134.

13 R. D. O. Silva, M. G. G. De Menezes, R. C. De Castro, C. D. A. Nobre, M. A. L. Milhome and R. F. Do Nascimento, Efficiency of ESI and APCI ionization sources in LC-MS/MS systems for analysis of 22 pesticide residues in food matrix, *Food Chem.*, 2019, **297**, 124934.

14 M. Murcia-Morales, V. Cutillas and A. R. Fernández-Alba, Supercritical fluid chromatography and gas chromatography coupled to tandem mass spectrometry for the analysis of pyrethroids in vegetable matrices: a comparative study, *J. Agric. Food Chem.*, 2019, **67**, 12626–12632.

15 J. Yao, Z. Wang, L. Guo, X. Xu, L. Liu, L. Xu, S. Song, C. Xu and H. Kuang, Advances in immunoassays for organophosphorus and pyrethroid pesticides, *TrAC, Trends Anal. Chem.*, 2020, 116022.

16 M. Moloney, S. Tuck, A. Ramkumar, A. Furey and M. Danaher, Determination of pyrethrin and pyrethroid residues in animal fat using liquid chromatography coupled to tandem mass spectrometry, *J. Chromatogr. B: Anal. Technol. Biomed. Life Sci.*, 2018, **1077**, 60–70.

17 L. Chen, J. Fu, Q. Lu, L. Shi, M. Li, L. Dong, Y. Xu and R. Jia, Cross-linked polymeric ionic liquids ion gel electrolytes by in situ radical polymerization, *Chem. Eng. J.*, 2019, **378**, 122245.

18 C. Roth, T. Peppel, K. Fumino, M. Köckerling and R. Ludwig, The importance of hydrogen bonds for the structure of ionic liquids: single-crystal X-ray diffraction and transmission and attenuated total reflection spectroscopy in the terahertz region, *Angew. Chem., Int. Ed. Engl.*, 2010, **49**, 10221–10224.

19 K. H. Hu, H. W. Zhang, M. K. Kong, M. Y. Qin, M. Ouyang, G. W. Wang and L. H. Zhuang, Effect of alkyl chain length of imidazolium cations on foam properties of anionic surface active ionic liquids: experimental and DFT studies, *J. Mol. Liq.*, 2021, **340**, 117197.

20 M. Shukla, Spectroscopic and DFT Studies of cation-anion interaction in imidazolium and piperidinium based ionic liquids, *J. Sci. Technol. Res.*, 2018, **8**, 5–11.

21 R. Phadagi, S. Singh, H. Hashemi, S. Kaya, P. Venkatesu, D. Ramjugernath, E. E. Ebenso and I. Bahadur, Understanding the role of dimethylformamide as co-solvents in the dissolution of cellulose in ionic liquids: experimental and theoretical approach, *J. Mol. Liq.*, 2021, **328**, 115392.

22 Z. Liu, S. Z. E. Abedin and F. Endres, Raman and FTIR spectroscopic studies of 1-ethyl-3-methylimidazolium trifluoromethylsulfonate, its mixtures with water and the solvation of zinc ions, *ChemPhysChem*, 2015, **16**, 970–977.

23 Y. Z. Zheng, N. N. Wang, J. J. Luo, Y. Zhou and Z. W. Yu, Hydrogen-bonding interactions between $[BMIM]BF_4$ and acetonitrile, *Phys. Chem. Chem. Phys.*, 2013, **15**, 18055–18064.

24 Q. B. Zhang, C. Yang, Y. X. Hua, Y. Li and P. Dong, Electrochemical preparation of nanostructured lanthanum using lanthanum chloride as a precursor in 1-butyl-3-methylimidazolium dicyanamide ionic liquid, *Phys. Chem. Chem. Phys.*, 2015, **17**, 4701–4707.

25 M. S. Gruzdev, U. V. Chervonova, A. A. Ksenofontov, M. A. Krestianinov, A. I. Alexandrov and T. V. Pashkova, Schiff base complexes with different metals incorporating derivatives of 3,6-di-tert-butylcarbazole, *Appl. Organomet. Chem.*, 2021, **35**, e6145.

26 S. E. Lyubimov, E. A. Rastorguev and V. A. Davankov, The use of a new ionic phosphite ligand in the hydroformylation catalyzed by rhodium complexes: Effect of reaction media, *Russ. J. Phys. Chem. B*, 2014, **8**, 953–957.

27 X. Yang, M. Wang, J. Zhao, C. Cui, S. Wang and J. Liu, Multichromic polymers containing alternating bithiophenes derivatives and 4-cyanotriphenylamine unit and their application for electrochromic devices, *J. Electroanal. Chem.*, 2014, **714**, 1–10.

28 X. M. Ye, C. M. Shao, Q. H. Fan, L. R. Shang and F. F. Ye, Porous carbon nanotube microspheres with tailorable surface wettability areas for oil adsorption, *J. Colloid Interface Sci.*, 2021, **15**, 737–745.

29 S. Sadeghi and S. Oliaei, Microextraction of sulfathiazole from milk and honey samples using a polymeric ionic liquid membrane followed by fluorometric determination, *J. Food Compos. Anal.*, 2021, **97**, 103774.

30 Y. Zhang, H. Ding, Y. Wu, C. Zhang, B. Bai, H. Wang and M. Li, Ultrasound-induced controllable morphology and growth dimension in a dihydrazide-based self-assembly system, *Soft Matter*, 2014, **10**, 8838–8845.

31 D. Allen, Preparation and characterization of 1-butyl-3-methylimidazolium tetrafluoroborate ionic liquids, *J. Chem. Eng.*, 2013, **3**, 187–197.

32 K. Goossens, K. Lava, C. W. Bielawski and K. Binnemans, Ionic liquid crystals: versatile materials, *Chem. Rev.*, 2016, **116**, 4643–4807.

33 M. Galib and G. Hanna, The role of hydrogen bonding in the decomposition of H2CO3 in water: mechanistic insights from ab initio metadynamics studies of aqueous clusters, *J. Phys. Chem. B*, 2014, **118**, 5983–5993.

34 J. A. Abia and R. Ozer, Development of polyoxometalate-ionic liquid compounds for processing cellulosic biomass, *Bioresources*, 2013, **8**, 2924–2933.

35 S. Zhang, J. Wang, X. Lu and Q. Zhou, *Structures and interactions of ionic liquids*, Springer, Berlin, 2013.

36 A. A. Tietze, H. Pascal, S. Annegret and I. Diana, Ionic liquid applications in peptide chemistry: synthesis, purification and analytical characterization processes, *Molecules*, 2018, **17**, 4158–4185.

37 Z. D. Ding, Z. Chi, W. X. Gu, S. M. Gu, J. H. Liu and H. J. Wang, Theoretical and experimental investigation on dissolution and regeneration of cellulose in ionic liquid, *Carbohydr. Polym.*, 2012, **89**, 7–16.

38 N. J. Brooks, F. Castiglione, C. M. Doherty, A. Dolan, A. J. Hill, P. A. Hunt, R. P. Matthews, M. Mauri, A. Mele and R. Simonutti, Linking the structures, free volumes, and properties of ionic liquid mixtures, *Chem. Sci.*, 2017, **8**, 6359–6374.

39 A. Mehrdad and M. Taleb-Abbasi, Viscometric behavior of hydroxyethyl cellulose in aqueous solutions of some imidazolium ionic liquids, *Cellulose*, 2019, **26**(13), 7685–7693.

40 S. Yesudass, L. O. Olasunkanmi, I. Bahadur, M. M. Kabanda, I. B. Obot and E. E. Ebenso, Experimental and theoretical

studies on some selected ionic liquids with different cations/anions as corrosion inhibitors for mild steel in acidic medium, *J. Taiwan Inst. Chem. Eng.*, 2016, **64**, 252–268.

41 L. A. Kartsova, E. A. Bessonova and E. A. Kolobova, Ionic liquids as modifiers of chromatographic and electrophoretic systems, *J. Anal. Chem.*, 2016, **71**, 141–152.

42 H. W. Cheng, J. N. Dienemann, P. Stock, C. Merola, Y. J. Chen and M. Valtiner, The effect of water and confinement on self-assembly of imidazolium based ionic liquids at mica interfaces, *Sci. Rep.*, 2016, **6**, 1–9.